ARTICLE

In situ Nanomechanical Research on Large-Scale Plastic Deformation of Individual Ultrathin Multi-walled Carbon Nanotube

Guo-xin Chen[a,b], Jun-feng Cui[a,c], Huan-ming Lu[a], Jin-hong Yu[a*], Yan Liu[a], He Li[a*], Nan Jiang[a*]

a. Key Laboratory of Marine Materials and Related Technologies, Zhejiang Key Laboratory of Marine Materials and Protective Technologies, Ningbo Institute of Materials Technology & Engineering, Chinese Academy of Sciences, Ningbo 315201, China
b. University of Chinese Academy of Sciences, Beijing 100049, China
c. Dalian University of Technology, Dalian 116023, China

(Dated: Received on December 18, 2018; Accepted on January 21, 2019)

Carbon nanotubes are a promising candidate for the application of flexible electronics due to the ultrahigh intrinsic conductivity and excellent mechanical flexibility. In the present work, the morphology of the ultrathin (diameter: <20 nm) multi-walled carbon nanotubes (MWCNTs) under an axial compression was investigated by using *in-situ* transmission electron microscopy. Moreover, the overall dynamic deformation processes and the force-displacement (*F-D*) curves of the MWCNTs were also examined. Interestingly, the MWCNTs almost restored their original morphology after 15 loading-unloading cycles. The deformation and recovery process indicate that the MWCNTs are flexible and exhibit excellent durability against compression. The Young's modulus of the MWCNTs is estimated with the value of ∼0.655 TPa derived from the *F-D* curves fitting. Our results suggest that the ultrathin carbon nanotube structures may have great application potentials in flexible devices.

Key words: Carbon nanotubes, *In-situ* transmission electron microscopy, Large-scale deformation, Young's modulus, *F-D* curve

I. INTRODUCTION

Flexible electronic devices have broad application prospects, such as various flexible displaying apparatus, flexible solar cells, flexible circuits, user friendly and portable biodetections, typically including skin-like pressure sensors and conformable RFID tags [1, 2]. Up to now, there have been several kinds of functional materials that are available for the fabrication of flexible electronic devices. Especially, carbon nanotubes (CNTs) composed of tubular carbon-based nanostructures, are a promising candidate for the application as flexible electronics that intrinsically result from the corresponding ultrahigh carrier mobility, conductive property in addition to excellent mechanical flexibility [3−5]. In recent years, the incorporation of CNTs and polymized materials has provided a promising and controllable strategy for the development of reinforced polymer films with uniform electronic properties through the morphological modification or electronic interaction methods [6−10]. In general, the combination of CNTs into host polymers can introduce additional energy levels or form carrier traps by selectively facilitating or blocking the transport of charge carriers, leading to the improvement of the OLED performance [11]. However, electrical conductance would be significantly changed with the mechanical strength of CNTs and sometimes even degenerated in practical application of the flexible electronic devices, due to the buckle of CNTs during actual use [12, 13]. Thus, the stiffness, flexibility, durability against mechanical compression, or stretching will be the basic criterion for assessment of the performed functionality and lifetime reliability for the CNT-based flexible electronic devices.

However, owing to the dimensions, it is a challenge to determine the mechanical properties of a single CNT. In the past decades, extensive researches in both experimental and theoretical aspects were investigated on mechanical performance of the CNTs, and it was revealed that the defect-free CNTs have extraordinary elastic moduli (0.27−1.47 TPa) and ultra high strength (10−66 GPa) [14−17]. Theoretical models that can derive the bending and bulking properties are presently constrained to a small sized CNTs with diameter of tens of nanometers [18]. Compared with the theoretical calculation approaches, experiments can give direct measurement results [19]. The elaborative manipulations within scanning probe microscopy were typically carried out to investigate the buckling instability as well as the mechanical properties of CNTs. Falvo *et al.* employed the tip under an atomic force microscope to investigate the behavior of CNTs under large strain. Their experi-

*Authors to whom correspondence should be addressed. E-mail: yujinhong@nimte.ac.cn, lihe@nimte.ac.cn, Jiangnan@nimte.ac.cn

mental investigations clearly revealed that the CNTs could be bent repeatedly without any catastrophic failure in a large range of bending angles [20]. Unfortunately, the unavoidable friction influence and torque induced by SPM cantilever tilt during the force measurement process, resulting in a high increment of the force distribution. To observe the geometry of CNTs, including the structure of the inner nanotubes, especially with atomic resolution, a transmission electron microscope (TEM) is necessary, by which the thermal vibrations of an individual CNT were measured and an elastic modulus of 1.8 TPa was firstly reported. Coincidentally, the Young's modulus of single-walled CNTs was determined by using the similar *in-situ* TEM method [21−23] with the value of 1.25 TPa. The modulus of ∼810 GPa was obtained for the structurally ordered muti-walled carbon nanotubes (MWCNTs) synthesized by the arc-discharge method. For the case of disordered CNTs synthesized by catalytic thermal decomposition, the detected elastic moduli were as low as 10−50 GPa. The irreversible buckling during bending process was ascribed to the unfavorable configurations as well as the fractures on the surface of CNTs [24]. The above experiments indicated the extremely high mechanical strength of several types of CNTs and demonstrated the fact that these properties depend on the size and structure of the CNTs.

Although extensive researches about the mechanical properties of CNTs have continued for over ten years, there have not been any experimental parameters reported up to date on the durability for an individual CNT under compression. To reveal and evaluate the durability under compression, the load displacement responses as well as the morphology evolution are investigated in this work, by pressing the individual CNTs continuously with multiple loading cycles through an *in situ* TEM method. Among various CNTs, ultrathin MWCNTs (diameter: <20 nm) may be more suitable for strengthening structural materials in addition to many more functional applications, especially for the cases applied in the situations via compressive stress and/or repeated bending. Although there are many characterization aspects of CNTs, there are few results reported in literature on the comparative study on buckling morphologic and/or structural evolution for the ultrathin MWCNTs, especially on large deformation under axial compression. Herein, we performed an *in situ* nanostructured mechanical investigation on the force-displacement features of a single MWCNT with large-scale deformation and mutiple loading cycles. The overall strain history of the detected CNTs will be displayed during the mechanical tests, including the initial states as well as the reversibility of the structure for the singular carbon nanotubes via taking the greatest advantage of the *in-situ* TEM technique.

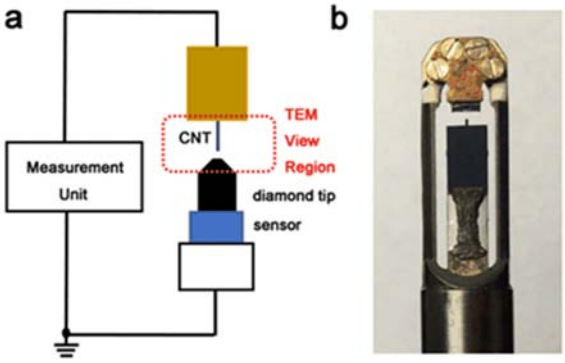

FIG. 1 (a) Schematic illustration of the experimental setup for *in-situ* nanoindentation. (b) Photograph of the initial position of MWCNTs against diamond tip that can be precisely adjusted with piezo-driven displacement in TEM experiment.

II. EXPERIMENTS

A. Materials Chemicals

The multi-walled carbon nanotubes (GT300, with purity of 97.5 wt%, average diameter of 12.9 nm, and length of 3−12 μm) prepared by chemical vapor deposition were purchased from Shandong Dazhan Nanomaterials Company Limited, China. The samples were further annealed at 2600 °C for 30 min in vacuum by a custom-made furnace.

B. Characterizations

Using the Renishaw spectrometer with a 532 nm laser excitation line, the Raman spectra were collected in a backscattering configuration. The diameter of the laser beam (with objective 50×) focused on the CNT, which was deposited on the Si/SiO_2 substrate, was approximately 1 μm. Raman spectra were collected at a resolution of 2 cm^{-1} between 1200 and 3000 cm^{-1}.

The CNTs were fixed on the side of poll to push (PTP) using a previous reported method [15]. A small amount of CNT powder was picked up by the eyebrow and then transferred to the PTP side which plays a role of the sample stage. The *in-situ* TEM experiments were realized by a dedicated piezoelectric driven STM holder (Hysitron PI-95), shown in FIG. 1(a). Under an optical microscope, the relative positions of the silicon and diamond tip were manually adjusted to a minimum possible gap distinguished by eye. After that, the final positions (X, Y, and Z) of the diamond tip and the target MWCNT were adjusted through the piezo-driven with nanoscale precision inside the TEM column. The motion and force acquisition parameters of the sample were programmed and controlled by special software and electronic devices. FIG. 1(b) presents a typical setup for *in situ* experimental nanoindentation. Carbon

DOI:10.1063/1674-0068/cjcp1812282

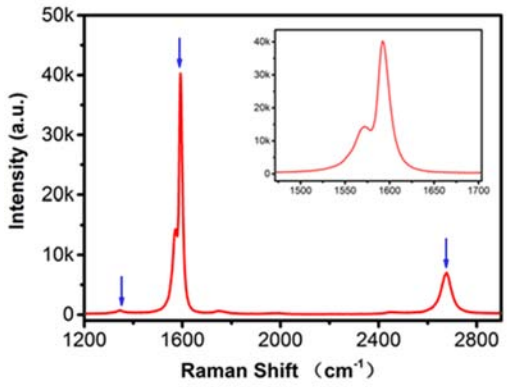

FIG. 2 Raman spectrum of the CNT sample.

nanotube perpendicular to the diamond tip was selected to perform the compression force applied along the axis. The designed micro capacitive sensor is performed relying on a piezoelectric actuator that can manuplicate a kind of indenter into the sample and have capability to measure the force-displacement curve directly. The test was conducted with a loading speed kept constant at 5 nm/s by using a displacement control.

All the experiments are performed inside a 200 kV TEM (FEI Tecnai F20) with a field-emission electron source. To record the sequential images, a Gatan894 CCD camera was used with the exposure time of 0.1 s, and the recording rate was 10 frame/s. The typical electron beam intensity during experiments was 0.5 A/cm^2 for both imaging and video recording. The experiment time was shortened, and low or medium magnification was utilized to record the images for the sake of avoiding the radiation and knockout damage.

III. RESULTS AND DISCUSSION

As the Raman spectrum shown in FIG. 2, the stretched graphitic C−C bonds which can be easily detected in the spectrum are attributed to the G-band Raman feature [25]. In detail, the magnified curve, as seen in the inset of FIG. 2 indicates that there are two main components of the G-band, G+ peak at 1590 cm^{-1} in addition to G− peak at ∼1570 cm^{-1}. According to the previous investigations, the G+ peak is associated with the longitudinal optical (LO) phonon mode for the carbon atom vibrations along the axis direction while the G− peak is related to the transverse optical (TO) phonon mode for C vibrations along the circumferential direction of the CNTs, respectively. The spectral shape indicates that the CNTs are a semiconducting type (Lorentz shape). The peak at 2675 cm^{-1} is attributed to G′ band for the CNTs, which corresponds to a typical sp^2 configuration detected in the graphitic materials. The observation of the G′ band in the sample emphasizes that the CNTs are of graphitic feature with a Raman-allowed mode for sp^2 carbons. Interestingly, the observation of a very small disorder-induced (D band) peak at 1347 cm^{-1} indicates a high-quality CNT sample after 2600 °C annealing.

In FIG. 3, it exhibits that the outer and inner diameter of the MWCNT is around 12.86 nm and 5.19 nm, respectively. Thus, the thickness of the CNT wall was estimated to be 3.84 nm, close to ∼11 layers, which is equivalent to the theoretic layers supposing that an inter-wall spacing is 0.34 nm [26]. For this study, two merits were provided by the selection of these CVD-grown NWs. Firstly, without using the FIB technique for the sample preparation, the Ga ion irradiation damage on the material's surface layer can be avoided [27], so that the intrinsic mechanical behavior of the material can be revealed. Secondly, CNT with diameter of 12.9 nm is possible to grow and be investigated. The size is below what can be fabricated using the FIB technique due to the current resolution limits in ion optics.

Only a few of experimental axial compression tests of MWCNTs have been carried out so far. The difficulties lie in the sample preparation, sample fixing, and the controlling of the nanomanipulator. The axial alignment of the sample can be verified by the *in situ* TEM. FIG. 4(a−h) shows a range of microscopy images as a function of time and the whole process can be found in the video in supplementary materials (Movie 1). FIG. 4(i) presents part of the corresponding force-displacement curve (from 0 s to 48 s). Points a−h in FIG. 4(i) correspond to the images in FIG. 4 (a−h), respectively. The diamond tip was moved from bottom to top, and then push and bend the carbon nanotube. It is clearly detected that the carbon nanotube started to bend at the bottom edge from the contacting area of the diamond tip, during the pushing movement [28].

When the diamond tip approaches the carbon nanotube, a slightly negative force of −3 nN is measured, which is caused by the attraction of electrostatic force between diamond tip and carbon nanotube. After marching forward ∼40 nm, the CNTs are touched by the diamond tip and suffer a compressive force. With the displacement of the punch increase continuously, the force increases linearly. From FIG. 4(c−e) (from 21 s to 32 s), a kink was formed as indicated by the red arrow. The kink indicates a large deformation of carbon nanotube but unfortunately its direction is parallel to the direction of the electron beam and thus its morphology cannot be seen. At the same time, a drop in force from 191 nN to 181 nN is observed, which is attributed to the occurrence of kink and some form of relaxation process [21].

Generally, when the CNTs possess small aspect ratio and they would undergo shell buckling but at the same time they keep a straight cylindrical axis; however, comparably the CNTs with thin and long geometry have a tend to illustrate sets of shell and column (or Euler) buckling [21]. Presumably, owing to the variation in shape, which is typically referred to a moment from inertia of area, the maximum compressive force

DOI:10.1063/1674-0068/cjcp1812282

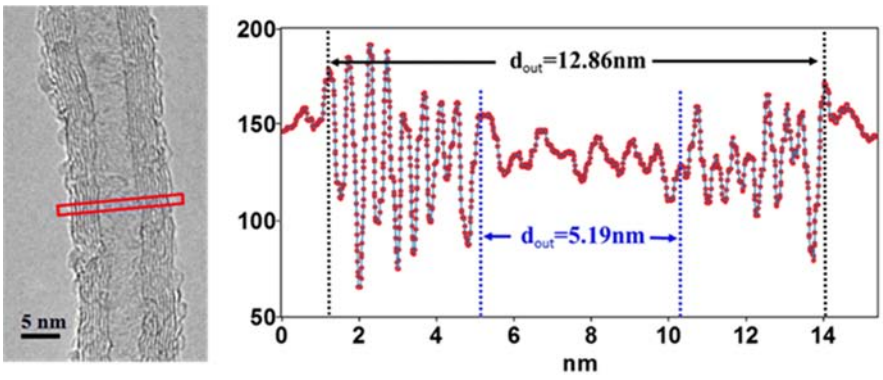

FIG. 3 Left panel: HRTEM image of a typical multi-walled carbon nanotube, right panel: histogram profile of the HRTEM.

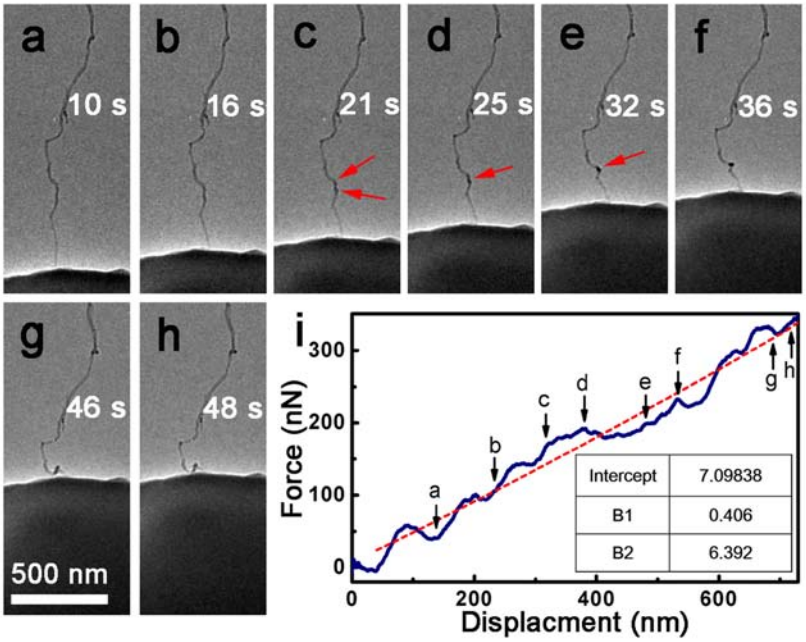

FIG. 4 (a−h) A series of microscopy images as a function of time at 10, 16, 21, 25, 32, 36, 46, and 48 s. (i) Part of the corresponding force-displacement curve. Points a−h in (i) correspond to the images in (a−h), respectively. The white scale bar in (g) represents 500 nm and all figures have the same scale.

in our experiment is larger than the reported data in literature for the buckling/kinking of the studied individual MWCNTs (100−101 nN) [21]. Fortunately, another kink like a "nanohook" of 42 nm curvature radius was then formed from 36 s to 48 s (FIG. 4(f−h)), the direction is perpendicular to the electron beam. The corresponding load is 232−342 nN where the diamond tip displacement is 532−728 nm. It should be noted that no fracture was seen and the diameter of the carbon nanotube did not change during this process. The maximum local strain on the outside tube surface is 29% which can be estimated from Eq.(1):

$$\varepsilon = \frac{\gamma_0}{\gamma_c} \tag{1}$$

where γ_0 is the tube radius, γ_c is radius of curvature of bend. It is astonishing that under such large-scale deformation the detected CNT presents apparent lack of catastrophic damage. The result could be deduced from the following two reasons relevant to the accommodated strain. Firstly, it is considered that there are dense defects in the MWNTs in significant concentration, especially for the case grown by CVD [26, 29]. The change of the geometry observed in the individual nanotube at the bend point implies that the detected MWCNTs suffer from shell buckling. The possible reason can be attributed to the incoherent of defects in this tube. As consequences, they separate or slide reversibly between neighboring layered carbon sheets as suffering the forces of tensile or compressive stress, respectively. Secondly, the deformation can also be tolerated within a large degree distortion of carbon sheets that are con-

DOI:10.1063/1674-0068/cjcp1812282

nected. Under certain conditions, the breaking strains could be as large as 30%, as shown in the report on the single-wall CNTs via molecular-dynamics [30]. In the researches of the mechanical behavior of ultrathin MWCNTs under strain, a similar result was also reported by Schaper *et al.* [31] and Tsai *et al* [32].

FIG. 5 presents a series of TEM images taken in the unloading process. Attributed to its hierarchical structure, the CNT showed a superior flexibility. When the diamond tip retracted from top to bottom, the CNT detected in the study could return to the corresponding original form and/or position without any noticeable structure change in the shape and geometry. These results indicate that the bending and bulking deformation of the CNT was predominantly elastic. Their deformation consisted of the constituent CNTs' alignment, and the C−C bonds' rotation and stretching [33]. Under the unloading process, the CNTs demonstrate a reversible deformation without any accelerated creation of interlinks by defects and interstitials in the kink area. The reason for the CNTs with such a reversible transition is resulted generally from the intrinsic properties of singular CNTs possessing impressively full recoverability based on the early investigations in Ref.[31].

Generally, according to Eq.(2), the stress, σ, for a homogeneous slender column can be named as a compression force. F is performed on the free end over the cross-section area of MWCNT (A) according to Eq.(2), which can be further expanded to Eq.(3), when the stress is approximated by the two order approximation. E in Eq.(3) is namely represented as Young's modulus, referring to homogeneous columns or rods only.

$$F = \sigma A \tag{2}$$

$$F = (E\varepsilon + D\varepsilon^2)A = \frac{EA}{L}\Delta L + \frac{DA}{L^2}(\Delta L)^2 \tag{3}$$

$$\kappa = B_1 = \frac{EA}{L} \tag{4}$$

where L is the length of CNT, ΔL is the change in length, B_1 is the slope of the fitting line, as shown in FIG. 4(i).

The F-D curve in FIG. 4(i) can be fitted with the formula y=Intercept+B_1x+B_2x^2+B_3x^3, where B_1 is 0.406. And then, the Young's modulus of CNTs can be obtained from the relationship between B_1 and E, A and L, as shown in Eq.(4). Finally, the value can be determined as about 0.655 TPa based on the formula above. As estimated, the resulted data are much larger than the value of 0.456 TPa for a thick individual multi-walled CNT reported in Ref.[24].

In order to further verify the durability against mechanical compression, the carbon nanotube was subjected to fifteen cyclic loading. The testing was conducted under the same condition and the corresponding images are shown in FIG. 6. FIG. 6(f) presents part of the corresponding force-time curve. Surprisingly, in the

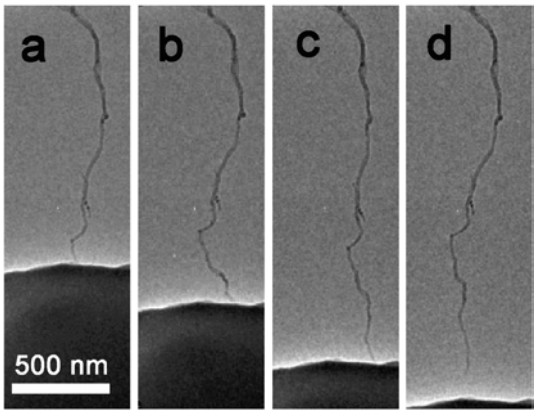

FIG. 5 Real-time TEM images showing morphology on unloading process of the individual MWCNT. All figures are at the same scale.

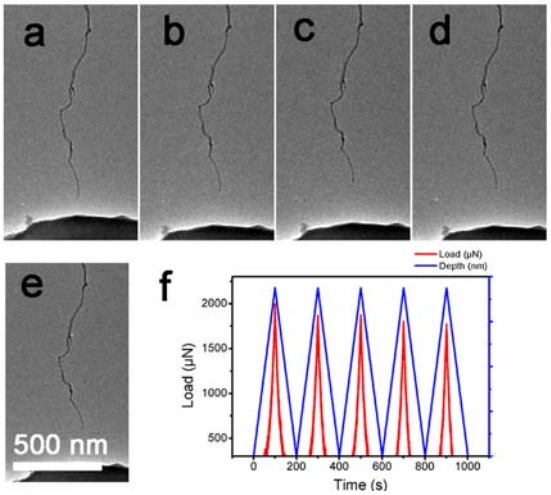

FIG. 6 (a−e) Real-time TEM images of after 11, 12, 13, 14, 15 loading-unloading cycles respectively and (f) the corresponding loading-unloading curve.

structural behavior between initial and after the cyclic loading on the nanotube, there was not any marked defect formation or destructive failure. Therefore, the reversible bending process was repeatable even after 15 cyclic loading. For the 11−15 cyclic loading, the maximum forces are 1992, 1863, 1811, and 1775 nN, respectively. The maximum force 2015 nN was compared to the first load, and the maximum force decreased by 11.9% after 15 cyclic loading. The MWCNTs show good durability under compression.

IV. CONCLUSION

The morphology change under the axis compression of an individual MWCNT has been investigated by *in-situ* TEM observations. Our investigation shows that the MWCNT undergoes large deformation. The Young's modulus for the detected individual MWCNT

DOI:10.1063/1674-0068/cjcp1812282

could be determined as about 0.655 TPa from the *F-D* curve. The carbon nanotube almost restored their original morphology after 15 loading-unloading cycles and the maximum force decreased by 11.9% compared to the first loading. The deformation and reversible process indicate that the carbon nanotubes are flexible and exhibit excellent durability against compression. It is suggested that the ultra-thin carbon nanotube structures have potential prospects in flexible devices application.

Supplementary materials: Movie 1 shows the overall dynamic structure evolution of an individual CNT under the axial compression and unloading process in the *in situ* TEM experiment.

V. ACKNOWLEDGMENTS

This work was supported by the National Natural Science Foundation of China (No.51573201, No.21773205, No.51501209, and No.201675165), NSFC-Zhejiang Joint Fund for the Integration of Industrialization and Informatization (U1709205), National Key R&D Program of China (2017YFB0406000), the Project of the Chinese Academy of Sciences (YZ201640 and KFZD-SW-409), Public Welfare Project of Zhejiang Province (2016C31026), Science and Technology Major Project of Ningbo (2016B10038 and 2016S1002), International S&T Cooperation Program of Ningbo (2017D10016), the 3315 Program of Ningbo, and the Science and Technology Major Project of Ningbo (2015S1001).

[1] S. Park, M. Vosguerichian, and Z. Bao, Nanoscale **5**, 1727 (2013).
[2] B. Kan, J. Ding, N. Yuan, J. Wang, Z. Chen, and X. Chen, Nanoscale Res. Lett. **5**, 1144 (2010).
[3] Q. Cao and J. A. Rogers, Adv. Mater. **21**, 29 (2009).
[4] L. Hu, D. S. Hecht, and G. Gruner, Chem. Rev. **110**, 5790 (2010).
[5] N. Rouhi, D. Jain, and P. J. Burke, ACS Nano **5**, 8471 (2011).
[6] D. Bikiaris, Materials **3**, 2884 (2010).
[7] Q. Sultana, M. Hasan, S. Iqbal, I. Shabib, A. Mitra, and M. Khan, Fibers **5**, 42 (2017).
[8] Y. Zhang, J. Fang, J. Li, Y. Guo, and Q. Wang, Polymers **9**, 728 (2017).
[9] S. C. Her and P. C. Chien, Materials (Basel) **10**, 408 (2017).
[10] L. Cai and C. Wang, Nanoscale Res. Lett. **10**, 1013 (2015).
[11] D. Zhang, K. Ryu, X. Liu, E. Polikarpov, J. Ly, M. E. Tompson, and C. Zhou, Nano Lett. **6**, 1880 (2006).
[12] J. Pan, S. Liu, Y. Yang. and J. Lu, Nanomaterials **8**, (2018).
[13] J. Yoon, J. Lee. and J. Hur, Nanomaterials **8**, 541 (2018).
[14] M. Yu, O. Lourie, M. J. Dyer, K. Moloni, T. F. Kelly, and R. S. Ruoff, Science **287**, 637 (2000).
[15] [15] M. F. Yu, B. S. Files, S. Arepalli, and R. S. Ruoff, Phys. Rev. Lett. **84**, 5552 (2000).
[16] B. G. Demczyk, Y. M. Wang, J. Cumings, M. Hetman, W. Han, A. Zettl, and R. ORitchie, Mater. Sci. Eng. A **334**, 173 (2002).
[17] W. Ding, L. Calabri, K. M. Kohlhaas, X. Chen, D. A. Dikin, and R. S. Ruoff, Exp. Mech. **47**, 25 (2007).
[18] Y. C. W. Shin-Pon Ju, and T. W. Lien, Nanoscale Res. Lett. **6**, 1 (2011).
[19] S. K. Jeon, H. S. Jang, O. H. Kwon, and S. H. Nahm, Nano Converg. **3**, 29 (2016).
[20] M. R. Falvo, G. J. Clary, R. M. I. Taylor, V. Chi, F. P. Brooks Jr., S. Washburn, and R. Superfine, Nature **389**, 582 (1997).
[21] K. Jensen, W. Mickelson, A. Kis, and A. Zettl, Phys. Rev. B **76**, 195436 (2007).
[22] J. Zhao and J. Zhu, Micron **42**, 663 (2011).
[23] H. Kohno and Y. Masuda, Appl. Phys. Lett. **106**, 193103 (2015).
[24] J. Zhao, M. R. He, S. Dai, J. Q. Huang, F. Wei, and J. Zhu, Carbon **49**, 206 (2011).
[25] M. S. Dresselhaus, G. Dresselhaus, R. Saito, and A. Jorio, Phys. Rep. (2005).
[26] O. Zhou, R. M. Fleming, D. W. Murphy, C. H. Chen, R. C. Haddon, A. P. Ramirez, and S. H. Glarum, Science **263**, 1744 (1994).
[27] V. Samaeeaghmiyoni, H. Idrissi, J. Groten, R. Schwaiger, and D. Schryvers, Micron **94**, 66 (2017).
[28] H. Kohno and Y. Masuda, Appl. Phys. Lett. **106**, 56 (2015).
[29] H. Jackman, P. Krakhmalev, and K. Svensson, J. Appl. Phys. **117**, 084318 (2015).
[30] B. I. Yakobson, M. P. Campbell, C. J. Brabec, and J. Bernholc, Comp. Mater. Sci. **8**, 341 (1997).
[31] A. K. Schaper, M. S. Wang, Z. Xu, Y. Bando, and D. Golberg, Nano Lett. **11**, 3295 (2011).
[32] P. C. Tsai and Y. R. Jeng, Mater. Sci. Eng. A **658**, 389 (2016).
[33] Z. Qin, X. Q. Feng, J. Zou, Y. Yin, and S. W. Yu, Appl. Phys. Lett. **91**, 043108 (2007).

DOI:10.1063/1674-0068/cjcp1812282